ACS OMEGA

http://pubs.acs.org/journal/acsodf

Article

# Preparation and Performance of a Cu@PtCu/CNF Oxygen Reduction Catalyst Membrane by Electrospinning

Xiaoting Deng, Min Lao, Zhenqin Li, Shaofeng Yin,* Feng Liu,* Zhiyong Xie, and Yili Liang

Cite This: *ACS Omega* 2022, 7, 31502−31508

Read Online

ACCESS | Metrics & More | Article Recommendations

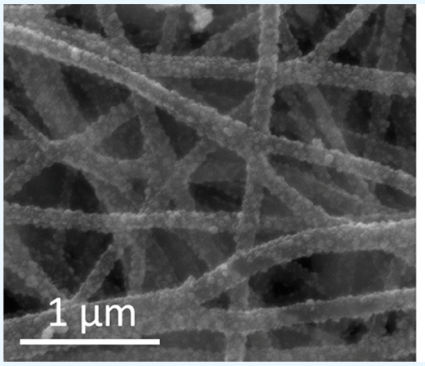


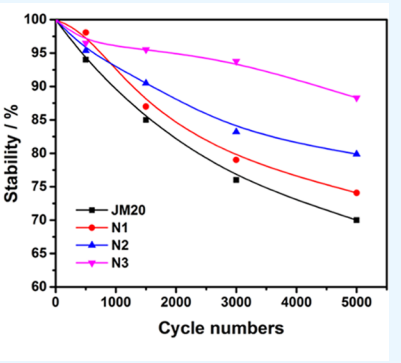


**ABSTRACT:** A flexible carbon nanofiber film with high conductivity was prepared by electrospinning, and then Cu was uniformly deposited on the fiber film by pulse electrodeposition to prepare Cu nanocrystal/carbon nanofiber film. Cu@PtCu/carbon nanofiber (Cu@PtCu/CNF) catalytic films were synthesized by in-situ substitution reduction. The Cu@PtCu/CNF catalytic film solves the problem of uneven activity of the catalytic layer and can be directly used as the catalytic layer. The morphology and structure were characterized by transmission electron microscopy (TEM), scanning electron microscopy (SEM), X-ray diffraction (XRD), and X-ray photoelectron spectroscopy (XPS). Electrochemical test results show that the Cu@PtCu/CNF catalytic films obtained at the chloroplatinic acid concentration of 0.5 mg·mL$^{-1}$ (N2) exhibited 2.5 times specific activity when compared with commercial Pt/C catalysts. After 5000 cycles of stability test, the electrochemical surface areas (ECSAs) were still maintained at 80%, and the half-wave potential decreased by 11 mV, which was better than those of commercial Pt/C catalysts.

## 1. INTRODUCTION

Proton-exchange membrane fuel cell (PEMFC) is a device that directly converts chemical energy into electrical energy, which can achieve zero pollution and zero emissions in the true sense.[1] Compared with the widely used lithium-ion battery, it has the advantages of short hydrogenation time and long cruising range. The membrane electrode (membrane electrode assembly, MEA) is the core component of the fuel cell. At present, the preparation method of the membrane electrode of the fuel cell is as follows: first, prepare the catalyst slurry; then, directly coat or transfer the slurry onto the proton membrane to obtain the catalyst/proton-exchange membrane module (named catalyst-coated membrane, CCM) and finally attach the gas dispersion layer to CCM to obtain membrane electrode (MEA).[2] In this process, the fuel cell catalyst must be an easily dispersible powder material, and it is difficult to achieve precise coordination of electrochemical reaction and mass transfer kinetics due to the "slurry" processing form of the catalytic layer.[3]

Electrospinning can be used for large-scale preparation of nanostructured materials such as hollow nanotubes and porous nanofibers by adjusting the parameters of the spinning precursor solution, needle type, and spinning environment.[4] One-dimensional carbon materials such as carbon nanofibers (CNFs) and carbon nanotubes (CNTs) have long-range orientation, good electrical conductivity, high temperature resistance, corrosion resistance, and other properties.[5] They overlap each other to form a three-dimensional network. The structure provides a channel for the transmission of gas and liquid. The long-range continuous ultrathin nanofiber membrane is obtained by electrospinning, and then a carbon membrane is obtained through a certain carbonization treatment process. The catalyst is attached to the carrier fiber membrane to make a catalyst membrane, and the catalyst

Received: July 4, 2022
Accepted: August 15, 2022
Published: August 24, 2022

membrane and the proton-exchange membrane can be directly attached to form a CCM.[6]

The cost and stability of proton-exchange membrane fuel cells limit their commercial promotion, and improving the activity and durability of cathode platinum-based catalysts is the main challenge. To this end, many researchers have developed different methods and developed catalysts such as nonprecious metal catalysts,[7] alloyed catalysts, and core−shell structures.[8] Among them, alloying is an effective method that can not only reduce the expensive platinum loading but also increase its activity by changing the extranuclear electron density of atoms on the catalyst surface with other metals.[9]

The alloying of Pt-based catalysts can improve the activity of catalysts; at the same time, one-dimensional fibers can overlap each other to form a three-dimensional network structure, which is beneficial to the transport of gas, liquid, and electricity as a catalyst carrier.[10] In this study, carbon nanofiber membranes with specific structures were prepared by electrospinning, and Cu nanocrystals with reducibility and alloy structure with Pt were supported on the carbon membranes utilizing pulse electrodeposition. The deposition and distribution growth regulation process of Cu microcrystals on carbon films were studied, and then Cu@PtCu/carbon nanofiber catalytic films were prepared by the displacement method.

## 2. EXPERIMENTAL SECTION

**2.1. Chemicals.** Poly(acrylonitrile) (PAN, MW = 90 000), *N*,*N*-dimethylformamide (DMF), copper sulfate pentahydrate ($CuSO_4·5H_2O$), 5 wt % Nafion solution, and chloroplatinic acid ($H_2PtCl_6·6H_2O$) were purchased from Aladdin. Absolute ethyl alcohol ($C_2H_5OH$), nitric acid ($HNO_3$), potassium hydroxide (KOH), and perchloric acid ($HClO_4$) were achieved from Sinopharm Chemical Reagent Co., Ltd. Commercial JM 20% Pt/C (JM 20) was purchased from JM Company. Ultrapure water was produced in our laboratory.

**2.2. Synthesis of Catalysts.** *2.2.1. Preparation of CNF Membrane.* The electrospinning method was used to prepare the PAN nanofiber membrane. First, 1.5 g of PAN was added to 13.5 g of DMF to prepare a polymeric precursor solution. Second, the precursor solution was loaded into a 10 mL syringe with a needle inner diameter of 0.41 mm ± 0.02 mm. The distance between the roller and the tip was set to 15 cm and the rotating speed was maintained at 500 rpm. The relative humidity was kept under 40% and the temperature was controlled between 35 and 40 °C. The feeding rate was 0.4 mL·h$^{-1}$ and the nanofibers (NFs) were collected by a piece of carbon paper under a high voltage of 20 kV. The PAN NFs membrane was stabilized for 6 h at 220 °C in an air oven and carbonized for 2 h at 1600 °C in Ar to prepare the CNF membrane.

*2.2.2. Synthesis of Cu/CNF Membrane.* Pulse electrodeposition was used to deposit Cu nanocrystals on the CNF membrane. The operation process was as follows: first, the working electrode was immersed in the $CuSO_4·5H_2O$ solution for 10 min to make the CNF membrane hydrophilic by electrochemical oxidation. Then, pulse electrodeposition was performed. Reverse pulse oxidation current density was set to 15 mA·cm$^{-2}$, while the pulse conduction time ($T_{on}$) and turn-off time ($T_{off}$) were 100 and 500 $\mu$s, respectively. The peak current density was −50 mA·cm$^{-2}$, and the pulse deposition time was 20 s. After that, the CNF membrane was quickly immersed in anhydrous ethanol for 10 min to avoid air oxidation. Finally, the membrane was washed with deionized water and dried in a vacuum drying oven at 50 °C to obtain the Cu/CNF membrane (Cu/CNFM).

*2.2.3. Synthesis of Cu@PtCu/CNF Membrane.* Cu/CNFM was immersed in the chloroplatinic acid solution for 1 h (the concentration was 0.25, 0.5, 1.0 mg·mL$^{-1}$, respectively), and the pH of the solution was adjusted to 4. The Cu@PtCu/carbon nanofiber membrane (Cu@PtCu/CNFM) was prepared by in situ chemical replacement. The membranes prepared with different concentrations (0.25, 0.5, 1.0 mg·mL$^{-1}$) of chloroplatinic acid solution were named N1, N2, and N3, respectively.

**2.3. Characterization of Catalysts.** The characterization of the samples was analyzed by scanning electron microscopy (SEM), transmission electron microscopy (TEM), high-resolution transmission electron microscopy (HRTEM), X-ray photoelectron spectroscopy (XPS), X-ray diffraction (XRD), and inductively coupled plasma (ICP). According to ICP results, the real content of Pt in N1, N2, N3, and Johnoson Matthey 20 (JM20) were 14.5, 19.3, 41.3, and 19.2 wt %, respectively. The real content of Cu in N1, N2, and N3 were 30.7, 19.3, and 12.3 wt %, respectively.

All of the electrochemical tests were carried out by a three-electrode system in 0.1 M $HClO_4$ solution at room temperature. For the preparation of catalyst ink, 2 mg of the electrocatalyst was mixed with 1.0 mL of water/isopropanol/Nafion (5 wt %) solution (volume ratios = 5:4:1), followed by sonication for 30 min. Then, 10 $\mu$L of the ink was dropped onto a rotating disk electrode (RDE, 5 mm diameter, 0.196 cm$^2$) using as a working electrode. A Pt sheet (1 cm × 1 cm) and a reversible hydrogen electrode (RHE) electrode were used as the counter electrode and the reference electrode, respectively. After saturating the solution with oxygen, cyclic voltammetry (CV) test was performed in the potential ranging from 0.05 to 1.20 V at 10 mV·s$^{-1}$. Linear sweep voltammetry (LSV) tests were performed at 20 mV·s$^{-1}$. The accelerated degradation test (ADT) was performed in the range of 0.6−1.1 V at a scan rate of 100 mV·s$^{-1}$. The commercial JM20 catalyst was measured through the same process to make a comparative analysis.

The electrochemical surface areas (ECSAs) of the catalysts were obtained by calculating the hydrogen adsorption peak area equation

$$\mathrm{ECSA} = Q_H/(210 \times \mathrm{Pt_{load}}) \quad (1)$$

where $Q_H$ is the charge for $H_2$ adsorption from 0.05 to 0.4 V vs RHE.[11]

The kinetic current density ($j_k$), mass activity (MA), specific activity (SA) can be calculated by the following equation

$$1/j = 1/j_k + 1/j_d \quad (2)$$

where $j$ is the measured current density and $j_d$ is the measured limiting current density.[12]

$$\mathrm{MA} = j_k/\mathrm{Pt_{load}} \quad (3)$$

$$\mathrm{SA} = \mathrm{MA}/\mathrm{ECSA} \quad (4)$$

## 3. RESULTS AND DISCUSSION

Figure 1a shows that the prepared membrane has a smooth surface and can be bent at a right angle, which indicates the flexibility of the CNF membrane. Figure 1b shows that carbon nanofibers are continuous in the long range and can be interlinked to form a three-dimensional network structure, which is conducive to the transmission of gas, liquid, and



https://doi.org/10.1021/acsomega.2c04187
ACS Omega 2022, 7, 31502−31508

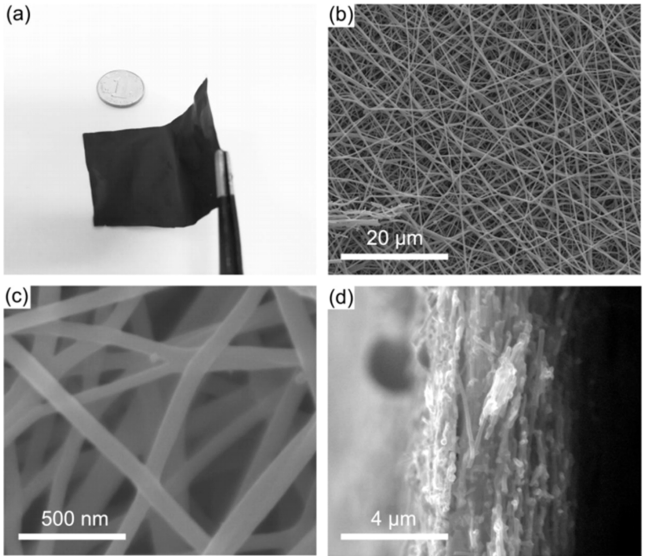


**Figure 1.** (a) Optical photograph, (b, c) SEM images, and (d) cross-sectional SEM images of CNF membrane carbonized at 1600 °C.

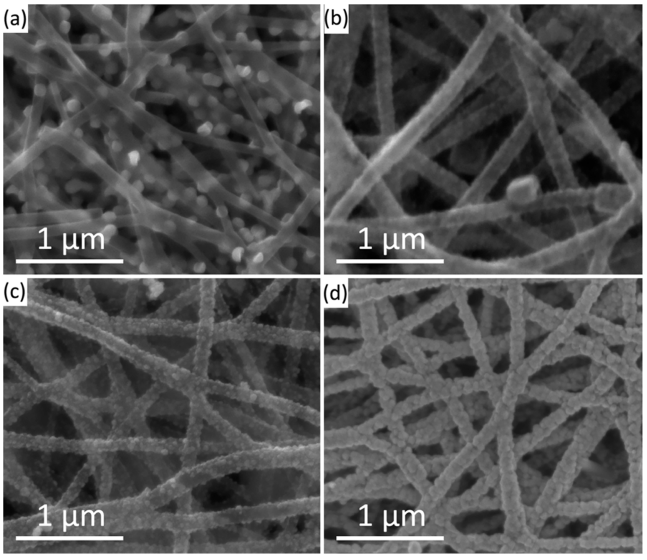


**Figure 2.** SEM images of (a) Cu/CNFM, (b) N1, (c) N2, and (d) N3.

electricity. Figure 1c shows that the fibers are about 150 nm in diameter, providing a large surface area to support the active material. Figure 1d shows that the cross-sectional thickness of the fiber membrane is about 4 $\mu$m, and its use as an integrated catalytic membrane is conducive to reducing the transport distance between the reactants and products, thus reducing the concentration polarization.

Figure 2 shows the morphology of Cu/CNFM and Cu@PtCu/CNFM prepared by different concentrations of chloroplatinic acid. The SEM images show that with the increase in the concentration of chloroplatinic acid, the metal particle coverage rate on the fiber surface increases, and the fiber surface becomes rougher. The increase in the concentration of the $Pt^{4+}$ can accelerate the replacement reaction, thus increasing the Pt-loading capacity on the fiber surface.

Figure 3 shows TEM images at different multiples and high-resolution lattice images of Cu@PtCu/CNFM (N2) and commercial catalyst JM20. Figure 3a shows that the surface of each fiber is uniformly covered with metal particles of uniform

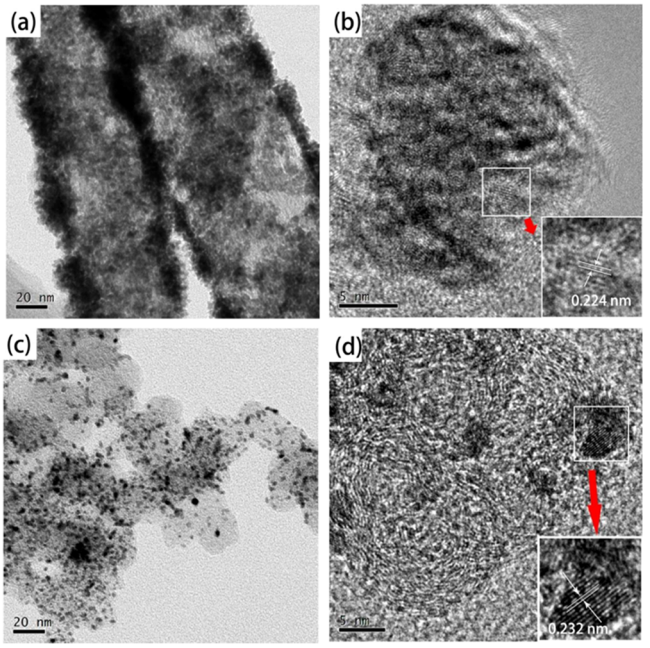


**Figure 3.** (a) TEM image and (b) HRTEM image of Cu@PtCu/CNFM. (c) TEM image and (d) HRTEM image of JM20.

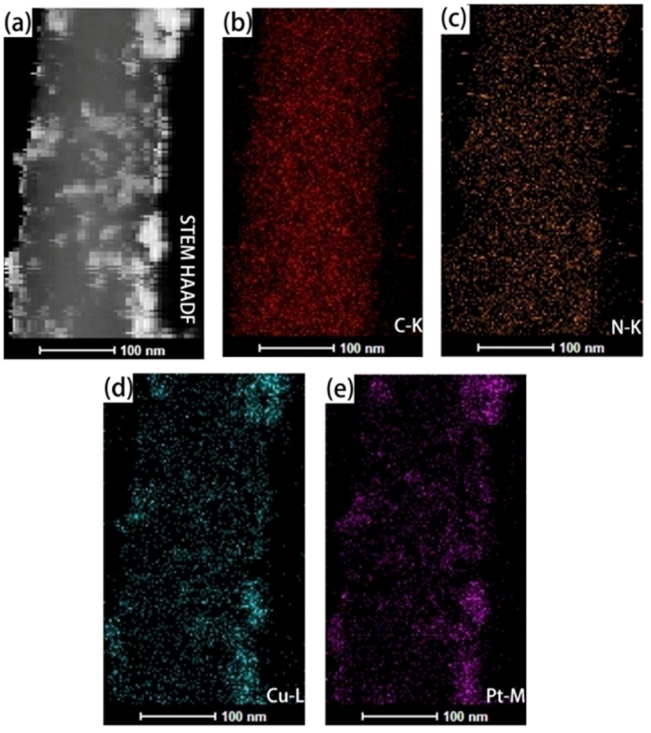


**Figure 4.** (a) High-angle annular dark field scanning transmission electron microscopy (HAADF-STEM) images of Cu@PtCu/CNFM, (b) C, (c) N, (d) Cu, and (e) Pt.

size, and some of them are distributed in clusters. As shown in Figure 3b, the lattice spacing is measured at about 0.222−0.224 nm. Compared with the crystal plane spacing of the pure Pt catalyst JM20 (0.232 nm), its crystal lattice shrinks, and it is closer to the (111) plane crystal spacing of the PtCu alloy of 0.2191 nm,[13] which indicated the formation of the PtCu alloy.

The element distribution of Cu@PtCu/CNFM was analyzed by mapping. As shown in Figure 4, Cu and Pt are uniformly



https://doi.org/10.1021/acsomega.2c04187
ACS Omega 2022, 7, 31502−31508

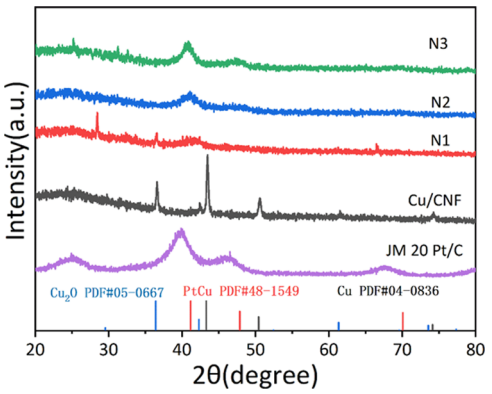


**Figure 5.** XRD spectra of N1, N2, N3, Cu/CNFM, and JM20.

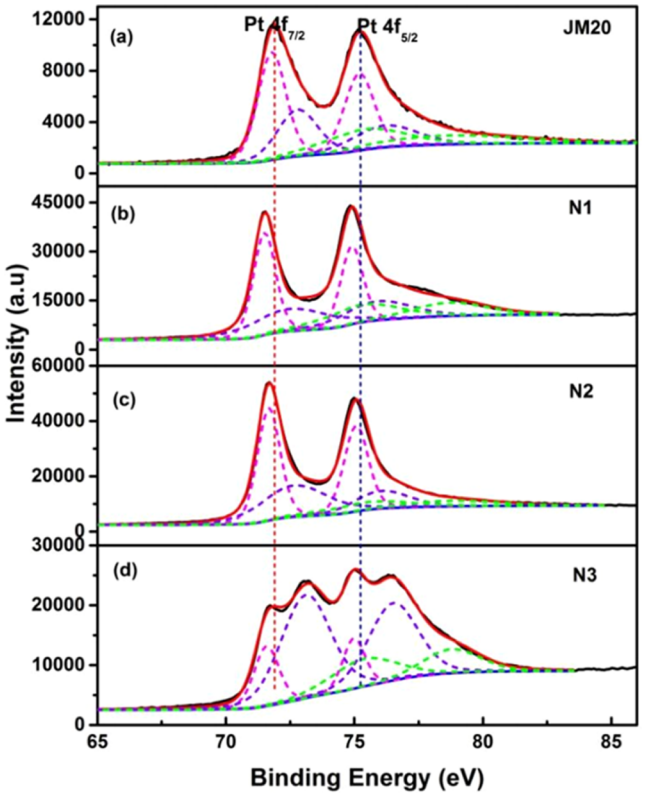


**Figure 6.** Pt 4f spectra of (a) JM20, (b) N1, (c) N2, and (d) N3.

**Table 1. Pt 4f in XPS Spectra**

| | Pt(0) (%) | Pt(II) (%) | Pt(IV) (%) |
|---|---|---|---|
| JM20 | 53.35 | 36.78 | 9.88 |
| N1 | 42.64 | 32.43 | 24.92 |
| N2 | 52.40 | 34.45 | 13.15 |
| N3 | 17.68 | 60.70 | 21.62 |

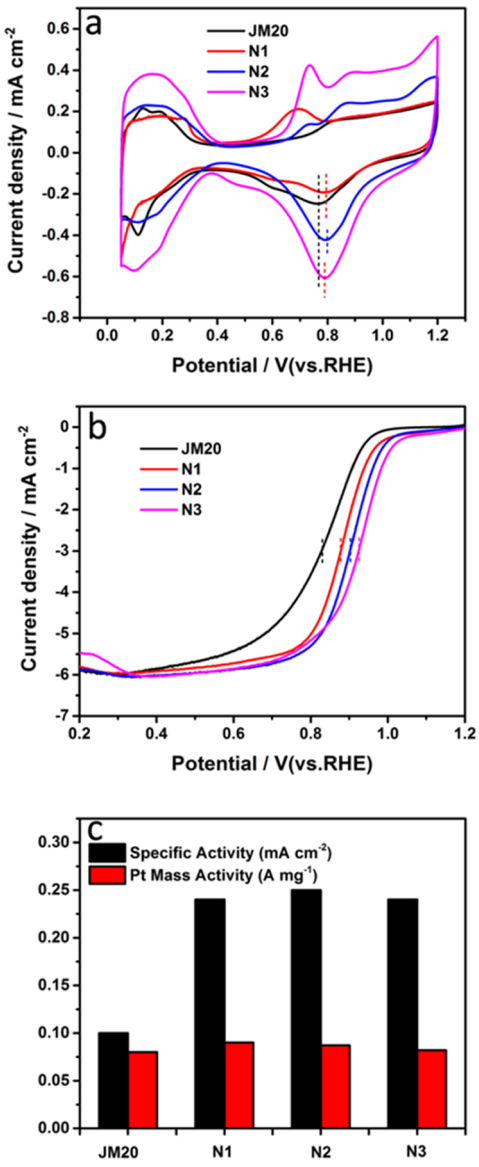


**Figure 7.** (a) CV curves and (b) LSV curves of JM20, N1, N2, and N3. (c) Bar graph of SA and MA of JM20, N1, N2, and N3.

**Table 2. Electrochemical Properties of JM20, N1, N2, and N3**

| | ECSA ($m^2 \cdot g^{-1}$) | $E_{on}$ (V) | $E_{1/2}$ (V) | SA@0.9 V ($mA \cdot cm^{-2}$) | MA@0.9 V ($A \cdot mg^{-1}$) |
|---|---|---|---|---|---|
| JM20 | 84 | 0.950 | 0.826 | 0.10 | 0.080 |
| N1 | 36 | 0.953 | 0.873 | 0.24 | 0.090 |
| N2 | 37 | 0.978 | 0.900 | 0.25 | 0.087 |
| N3 | 34 | 1.000 | 0.918 | 0.24 | 0.082 |

distributed on the fibers and their locations coincide, indicating that the PtCu alloy structure is formed in the shell layer. The carbon serves as catalyst support and is doped with nitrogen harmoniously. The nitrogen is mainly derived from PAN in the precursor solution.

Figure 5 compares the XRD spectra of N1, N2, N3, and Cu/CNFM. The characteristic peak of Cu@PtCu/CNFM at 41.1 and 47.8° corresponds to the (111) and (200) crystal planes of PtCu alloy.[14] In addition, with the increase in the concentration of $Pt^{4+}$, the characteristic peak of PtCu in the XRD pattern becomes sharp, indicating that the grain size increases due to the high concentration of $Pt^{4+}$, which easily reduces the active surface area of the catalyst. In addition, the characteristic peak of the copper oxide facies phase in N1 indicates that the oxide layer on the surface of copper nanocrystals cannot be removed under the low concentration of chloroplatinic acid. However, when the concentration of chloroplatinic acid increases to 0.5 $mg \cdot mL^{-1}$, the characteristic peak of the copper oxide disappears, indicating that the increase in the concentration of chloroplatinic acid is conducive to the etching of Cu oxide.



https://doi.org/10.1021/acsomega.2c04187
ACS Omega 2022, 7, 31502−31508

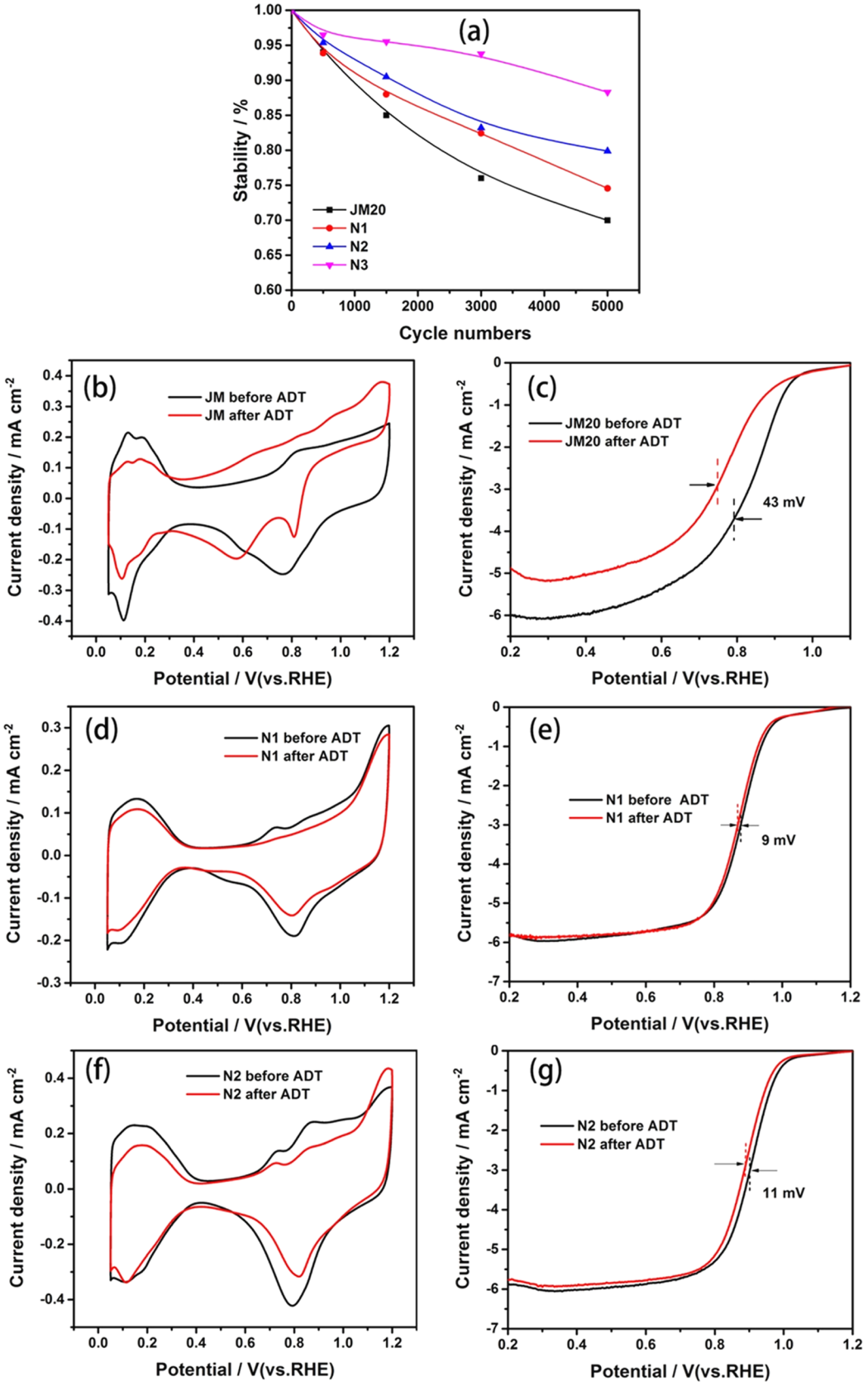


**Figure 8.** continued



https://doi.org/10.1021/acsomega.2c04187
*ACS Omega* 2022, 7, 31502−31508

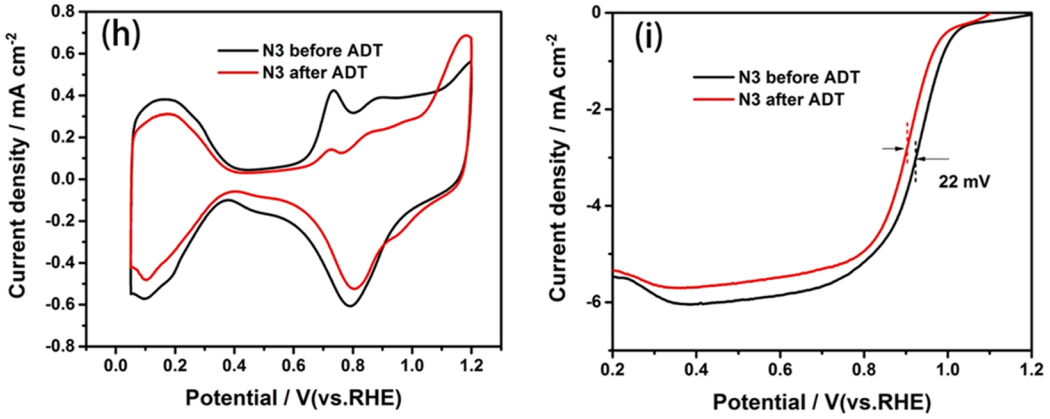


**Figure 8.** (a) ECSA/ECSA$_0$ of JM20, N1, N2, and N3. CV curves before and after ADT: (b) JM20, (d) N1, (f) N2, and (h) N3. LSV curves before and after ADT: (c) JM20, (e) N1, (g) N2, and (i) N3.

To characterize the chemical valence state of Pt in different electrocatalysts, XPS was performed. The result shows that the Pt 4f$_{7/2}$ of N1 (71.54 eV) and N2 (71.59 eV) samples shift toward lower binding energy relative to JM20 (71.95 eV) (Figure 6). This is because the formation of an alloy structure of Pt and Cu changes the electronic structure on the surface of the active substance. The transfer of the Cu surface electron to the Pt surface can enhance the peak potential of oxygen reduction and inhibit the oxidation of Pt, which is conducive to the positive regulation of catalytic activity of the catalyst.[14b] The fitting data of different states of Pt is shown in Table 1. Among them, the increase in Pt(0) is generally beneficial to the improvement in catalytic activity. Table 1 shows that the Pt(0) content of N1 is less than that of N2, and its Pt(IV) content is higher, indicating that the reduction degree of Pt in N1 is not as high as that of Pt in N2, and Pt is more attached to the membrane surface in the form of ion adsorption. This is due to the fact that some Cu nuclei oxide layers are not eroded and opened under N1 concentration (discussed in XRD analysis), which reduces the reduction degree of Pt. However, when the concentration is too high (N3), the content of Pt(0) decreases instead, which may be due to the consumption of large amounts of Cu nanocrystalline nuclei in the early stage of the replacement reaction. The replaced Pt constantly covers the surface of Cu nanocrystals, which slows down the reaction in the later stage and makes it difficult to reduce the adsorbed Pt$^{4+}$.

It can be seen from Figure 7 that the *OH adsorption peaks of N1 (0.809 V), N2 (0.803 V), and N3 (0.792 V) have a positive shift relative to JM20 (0.766), which reflects that they have a lower chemical adsorption energy for *OH. This is conducive to the increase in oxygen reduction activity. The ECSA results calculated by normalization are shown in Table 2. The table shows that the ECSA of JM20 (84 m$^2$·g$^{-1}$) is higher than that of N1 (36 m$^2$·g$^{-1}$), N2 (37 m$^2$·g$^{-1}$), and N3 (34 m$^2$·g$^{-1}$), which is due to the smaller diameter of active nanometal particles of JM20. It is worth mentioning that the CV curve of N2 does not have the oxidation peak of Cu crystals at 0.25 V, indicating that the shell structure formed in the PtCu alloy has good coverage of the internal Cu, which can effectively prevent the loss of Cu cores and help maintain its activity during the operation.

The electrochemical properties of each sample are shown in Table 2. It shows that the onset potential ($E_{on}$) and the half-wave potential ($E_{1/2}$) of the as-prepared catalysts are higher than that of JM20. Meanwhile, the values of MA of N1 (0.090 A·mg$^{-1}$), N2 (0.087 A·mg$^{-1}$), and N3 (0.082 A·mg$^{-1}$) are higher than that of JM20 (0.080 A·mg$^{-1}$). Among them, the electrochemical properties of N2 are the best, and the excellent performance of the sample can be explained by the appropriate Pt−Cu ratio, which can increase the electron-donating ability of Pt nanoparticles and promote the ORR process.

The electrochemical stability of a catalyst is an important index. The decreasing trend of the ECSA calculated for JM20, N1, N2, and N3 catalysts is shown in Figure 8. It shows that the ECSA of each sample decreases during ADT. The ECSA values of self-made catalysts decreased by 26, 19, and 12%, respectively, lower than that of JM20 (29%). The best durability of N3 may be due to the low reducibility of Pt on the N3 surface (as analyzed in XPS), which can be reduced in the cyclic stability test and partially offset the negative effects caused by Ostwald ripening. Figure 8 shows the CV curves and LSV curves of JM20, N1, N2, and N3 before and after 5000 cycles. After 5000 cycles, the $E_{1/2}$ of N1, N2, and N3 shifted negatively by 9, 11, and 22 mV, respectively, lower than that of JM20 (43 mV), and the CV curves of N1 and N2 coincide well with those before the cycles, indicating the better stability of N1 and N2, which is beneficial to its application in practical fuel cells. However, the decline in $E_{1/2}$ of N3 is relatively large, which may be because the lack of Cu made it difficult to form an alloy structure at this stage.

## 4. CONCLUSIONS

The Cu@PtCu/CNFM prepared at the concentration of 0.5 mg·mL$^{-1}$ chloroplatinic acid has the best catalytic performance, with the mass specific activity 1.125 times and the area specific activity 2.5 times as much as those of JM20, and has the best electrochemical stability. After 5000 cycles of ADT, its ECSA only dropped by 19%, better than those of commercial catalysts. This study provides a new method to prepare an integrated catalytic layer with high electrochemical performance.

## AUTHOR INFORMATION

### Corresponding Authors

**Shaofeng Yin** − *College of Food and Chemical Engineering, Shaoyang University, Shaoyang 422000, China*; Email: yinshaofeng2020@163.com

**Feng Liu** − *State Key Laboratory of Advanced Technologies for Comprehensive Utilization of Platinum Metals, Kunming Institute of Precious Metals, Kunming 650106, China*; Email: feng.liu@spmcatalyst.com



https://doi.org/10.1021/acsomega.2c04187
ACS Omega 2022, 7, 31502−31508

## Authors

**Xiaoting Deng** − *College of Food and Chemical Engineering, Shaoyang University, Shaoyang 422000, China;* orcid.org/0000-0003-0741-3513

**Min Lao** − *College of Food and Chemical Engineering, Shaoyang University, Shaoyang 422000, China*

**Zhenqin Li** − *National Key Laboratory of Science and Technology for National Defence on High-strength Structural Materials, Central South University, Changsha 410083, China*

**Zhiyong Xie** − *National Key Laboratory of Science and Technology for National Defence on High-strength Structural Materials, Central South University, Changsha 410083, China;* orcid.org/0000-0003-2520-9807

**Yili Liang** − *National Key Laboratory of Science and Technology for National Defence on High-strength Structural Materials, Central South University, Changsha 410083, China*

Complete contact information is available at: https://pubs.acs.org/10.1021/acsomega.2c04187


## Notes

The authors declare no competing financial interest.

## ■ ACKNOWLEDGMENTS

The authors acknowledge the financial support from the Hunan Provincial and Municipal Joint Fund Project (2022JJ50171) and the Open Project of State Key Laboratory of New Technologies for Comprehensive Utilization of Rare and Precious Metals (SKL-SPM-202003).

## ■ REFERENCES


(1) (a) Cruz-Martínez, H.; Rojas-Chávez, H.; Matadamas-Ortiz, P. T.; Ortiz-Herrera, J. C.; López-Chávez, E.; Solorza-Feria, O.; Medina, D. I. Current progress of Pt-based ORR electrocatalysts for PEMFCs: An integrated view combining theory and experiment. *Mater. Today Phys.* **2021**, *19*, No. 100406. (b) Liu, F.; Shi, L.; Lin, X.; Yu, D.; Zhang, C.; Xu, R.; Liu, D.; Qiu, J.; Dai, L. Site-density engineering of single-atomic iron catalysts for high-performance proton exchange membrane fuel cells. *Appl. Catal., B* **2022**, *302*, No. 120860.

(2) (a) Liu, Q.; Lan, F.; Chen, J.; Zeng, C.; Wang, J. A review of proton exchange membrane fuel cell water management: Membrane electrode assembly. *J. Power Sources* **2022**, *517*, 230723. (b) Bhosale, A. C.; Ghosh, P. C.; Assaud, L. Preparation methods of membrane electrode assemblies for proton exchange membrane fuel cells and unitized regenerative fuel cells: A review. *Renew. Sustainable Energy Rev.* **2020**, *133*, No. 110286. (c) Chen, D.; Pei, P.; Li, Y.; Ren, P.; Meng, Y.; Song, X.; Wu, Z. Proton exchange membrane fuel cell stack consistency: Evaluation methods, influencing factors, membrane electrode assembly parameters and improvement measures. *Energy Convers. Manage.* **2022**, *261*, No. 115651.

(3) Choi, S. R.; Lim, M.; Kim, D. Y.; An, W. Y.; Lee, S. W.; Choi, S.; Bae, S. J.; Yim, S.-D.; Park, J.-Y. Life prediction of membrane electrode assembly through load and potential cycling accelerated degradation testing in polymer electrolyte membrane fuel cells. *Int. J. Hydrogen Energy* **2022**, *47*, 17379−17392.

(4) Zhang, X.; Wang, L. Research progress of carbon nanofiber-based precious-metal-free oxygen reaction catalysts synthesized by electrospinning for Zn-Air batteries. *J. Power Sources* **2021**, *507*, No. 230280.

(5) (a) Remón, J.; Casales, M.; Gracia, J.; Callén, M. S.; Pinilla, J. L.; Suelves, I. Sustainable production of liquid biofuels and value-added platform chemicals by hydrodeoxygenation of lignocellulosic bio-oil over a carbon−neutral $Mo_2C$/CNF catalyst. *Chem. Eng. J.* **2021**, *405*, No. 126705. (b) Guan, J.; Chen, W.; Fang, Y.; Wang, L.; Fu, Y.; Guo, B.; Zhang, M. Electrospinning derivative fabrication of sandwich-structured CNF/$Co_3S_4$/$MoS_2$ as self-supported electrodes to accelerate electron transport in HER. *Int. J. Hydrogen Energy* **2022**, *47*, 14930−14941.

(6) Deng, X.; Yin, S.; Wu, X.; Sun, M.; Li, Z.; Xie, Z.; Liang, Y.; Huang, Q. Scalable preparation of PtPd/carbon nanowires in the form of membrane as highly stable electrocatalysts for oxygen reduction reaction. *Int. J. Hydrogen Energy* **2019**, *44*, 2752−2759.

(7) (a) Huang, S.; Ouyang, T.; Zheng, B.-F.; Dan, M.; Liu, Z.-Q. Enhanced Photoelectrocatalytic Activities for $CH_3OH$-to-HCHO Conversion on $Fe_2O_3$/$MoO_3$: Fe-O-Mo Covalency Dominates the Intrinsic Activity. *Angew. Chem., Int. Ed.* **2021**, *60*, 9546−9552. (b) Chen, C.; Wang, X.-T.; Zhong, J.-H.; Liu, J.; Waterhouse, G. I. N.; Liu, Z.-Q. Epitaxially Grown Heterostructured $SrMn_3O_6$−x-$SrMnO_3$ with High-Valence $Mn^{3+}/^{4+}$ for Improved Oxygen Reduction Catalysis. *Angew. Chem.* **2021**, *133*, 22214−22221.

(8) (a) Ma, N.; Wang, Y.; Zhang, Y.; Liang, B.; Zhao, J.; Fan, J. First-principles screening of Pt doped $Ti_2$CNL (N = O, S and Se, L = F, Cl, Br and I) as high-performance catalysts for ORR/OER. *Appl. Surf. Sci.* **2022**, *596*, No. 153574. (b) Gao, X.; He, L.; Yu, H.; Xie, F.; Yang, Y.; Shao, Z. The non-precious metal ORR catalysts for the anion exchange membrane fuel cells application: A numerical simulation and experimental study. *Int. J. Hydrogen Energy* **2020**, *45*, 23353−23367.

(9) Shroti, N.; Daletou, M. K. The Pt−Co alloying effect on the performance and stability of high temperature PEMFC cathodes. *Int. J. Hydrogen Energy* **2022**, *47*, 16235−16248.

(10) Deng, X.; Yin, S.; Xie, Z.; Gao, F.; Jiang, S.; Zhou, X. Synthesis of silver@platinum-cobalt nanoflower on reduced graphene oxide as an efficient catalyst for oxygen reduction reaction. *Int. J. Hydrogen Energy* **2021**, *46*, 17731−17740.

(11) Green, C. L.; Kucernak, A. Determination of the Platinum and Ruthenium Surface Areas in Platinum−Ruthenium Alloy Electrocatalysts by Underpotential Deposition of Copper. I. Unsupported Catalysts. *J. Phys. Chem. B* **2002**, *106*, 1036−1047.

(12) Deng, X.; Yin, S.; Wu, X.; Sun, M.; Xie, Z.; Huang, Q. Synthesis of PtAu/$TiO_2$ nanowires with carbon skin as highly active and highly stable electrocatalyst for oxygen reduction reaction. *Electrochim. Acta* **2018**, *283*, 987−996.

(13) Di, S.; Liu, W.; Guo, C.; Wang, F.; Bulanova, A.; Mebel, A.; Zhu, H. Hierarchical porous N-doped carbon-supported PtCu nanoparticles as an efficient catalyst for oxygen reduction reaction. *J. Power Sources* **2022**, *533*, No. 231270.

(14) (a) Alekseenko, A. A.; Pavlets, A. S.; Belenov, S. V.; Safronenko, O. I.; Pankov, I. V.; Guterman, V. E. The electrochemical activation mode as a way to exceptional ORR performance of nanostructured PtCu/C materials. *Appl. Surf. Sci.* **2022**, *595*, No. 153533. (b) Cui, S.-K.; Guo, D.-J. Microwave-assisted preparation of PtCu/C nanoalloys and their catalytic properties for oxygen reduction reaction. *J. Alloys Compd.* **2021**, *874*, No. 159869.